Theor Chem Acc (2006) 115: 161–169
DOI 10.1007/s00214-005-0055-3

REGULAR ARTICLE

E. Guàrdia · J. Martí · J.A. Padró

Ion solvation in aqueous supercritical electrolyte solutions at finite concentrations: a computer simulation study

Received: 30 May 2005 / Accepted: 1 July 2005 / Published online: 16 December 2005

Abstract A series of results from computer simulations of sodium chloride ionic solutions at both supercritical and ambient conditions are presented. We considered infinite dilute and finite concentration solutions ($m = 1, 2, 4$ mol kg^{-1}) at variable densities. Structure of water around ionic species is carefully analyzed. Special attention is devoted to the effects of ion pairing and clustering. Running coordination numbers and residence times of water molecules are also reported.

Keywords Electrolyte solutions · Finite concentrations · Supercritical water · Molecular dynamics simulations

1 Introduction

The study of electrolytes in aqueous solution is a central topic in a variety of fields, since ionic solutions in water are ubiquitous in nature and play a central role in industrial and environmental processes. As a few examples, the reader should mind the electrode processes [1], metal corrosion [2], oxidation of chemical and biochemical wastes [3] or microbiology [4]. From the experimental side, diverse techniques have been applied to gain knowledge of the underlying microscopic mechanisms of ion solvation and to understand the structure and dynamics of electrolyte solutions: electric field [5], calorimetry [6], conductimetric [7], infrared, Raman [8–10] and X-ray absorption spectroscopy measurements [11–13], neutron diffraction with isotopic substitution [14–16] and, more recently, non-linear femtosecond spectroscopy [17]. On the theoretical side, integral equation studies have been particularly important in the description of electrolyte solutions [18–20]. Studies of mean force potentials at infinite dilution [21] revealed the existence of several classes of ion pairing. So, together with the alkali–halide ion pair, the existence of ionic pairs of the same sign was revealed. The use of numerical calculations based on computer simulations have added lots of information. Most studies are performed at infinite dilution, at room [22–25], high temperature [26–28] or at supercritical states [29–33]. Other works are devoted to concentrated electrolyte solutions at ambient conditions [34–39] but, to our knowledge, few studies have been reported concerning supercritical aqueous ionic solutions at finite concentrations [40–44].

In particular, solute speciation in supercritical aqueous electrolyte solutions is relevant for diverse industrial and natural processes, such as corrosion of metals, solvent extraction or crystal growth. The presence of ionic species produces important modifications in both the structure and dynamics of water, mainly attributed to changes in the hydrogen bond (HB) network. When turning to supercritical conditions, water density may be experimentally controlled by pressure and temperature changes, varying the microscopic ambient in between liquid and gas-like environments. This produces, for instance, a remarkable reduction of the dielectric constant, which is reduced to only ∼6 in a typical supercritical regime. The microscopical cause of this changes is again the dynamical variation of the HB network. This is connected with the ability of supercritical water (SW) to dissolve nonpolar organic reactives and also explains the existence of separated contact ion pairs in low-density ambients. SW plays an important role in the oxidation of organic compounds, or as process water in some power generating complexes, to mention a few examples [45]. The main objective of this work is the study of ion solvation in aqueous electrolyte solutions at finite concentration in SW environments at several densities.

E. Guàrdia (✉)
Departament de Física i Enginyeria Nuclear,
Universitat Politècnica de Catalunya,
B4-205 Campus Nord, 08034 Barcelona, Catalonia, Spain
E-mail: elvira.guardia@upc.edu

J. Martí
Departament de Física i Enginyeria Nuclear,
Universitat Politècnica de Catalunya,
B5-206 Campus Nord, 08034 Barcelona, Catalonia, Spain
E-mail: jordi.marti@upc.edu

J.A. Padró
Departament de Física Fonamental, Universitat de Barcelona,
Diagonal 647, 08028 Barcelona, Catalonia, Spain
E-mail: japadro@ub.edu

2 Computational details

Molecular dynamics (MD) simulations of Na^+Cl^- in water at ambient ($T = 298\,K$, $\rho = 1\,gcm^{-3}$) and supercritical conditions have been carried out in order to study the influence of ionic concentration and water density on microscopic structure and dynamics. Supercritical states along the $T = 650\,K$ isotherm and very different densities have been considered. Ionic solutions at three concentrations ($m = 1, 2, 4\,mol\,kg^{-1}$) have been simulated and the results compared with those from MD simulations of single ions (Na^+ or Cl^-) in water ($m \sim 0$), which is a good approach to the infinite dilution conditions. The densities of the simulated systems have been obtained among the experimental data collected from Ref. [46] at room temperature and from Ref. [47] for the supercritical states. The values corresponding to $m = 4\,mol\,kg^{-1}$ have been fitted from the density differences with single polynomial functions. The experimental densities of the whole system (water+ions) as a function of the concentration are displayed in Fig. 1 and the numerical values used in the MD simulations systems are summarized in Table 1. States A, B, C and D correspond to the four isobaric lines plotted in Fig. 1.

The SPC/E rigid model has been assumed to model water–water interactions [48]. The molecular dipole moment of SPC/E water is $\mu = 2.35$ D and its critical point [49] is located at $T_c = 640\,K$, $\rho_c = 0.29\,g\,cm^{-3}$, $P_c = 160\,bar$. This point is very close to the experimental critical point of water, that is, $T_c = 647.13\,K$, $\rho_c = 0.322\,g\,cm^{-3}$, $P_c = 220.55\,bar$. The reliability of this model to accurately reproduce structural and dynamic properties of liquid water in a wide range of thermodynamic conditions has been previously established [50–52]. In particular, the calculated thermodynamic pressures have been observed to be in very good agreement with experimental values [52]. Ion-water forces have been modeled by means of Coulombic and 6–12 Lennard–Jones interaction potentials, the latter with the ϵ and σ parameters reported in Ref. [53]. These same parameters were also employed by several groups [31–33,54–56] to perform MD studies of ion-water solutions at room and high temperature conditions. With the same potential models, Brodholt [41] obtained values of the density very close to the experimental data for Na^+Cl^- in water at different temperatures and pressures close to the range analyzed in the present work. This gives an indication of the validity of the ion-water forces employed in this work to model supercritical ambients.

We employed a time step of 1 fs in all simulation runs. The length of equilibration runs was larger than 100 ps and simulation runs of more than 250 ps were employed to collect statistically meaningful properties. The simulated systems at finite concentration were composed of 864 water molecules plus several ion pairs (16, 32, 64 for the concentrations of $m = 1, 2, 4\,mol\,kg^{-1}$, respectively) placed in a cubic box, with box lengths appropriately chosen for each density considered. In the case of the infinite dilute solutions ($m \sim 0$) the systems were made up by a single ion and 256 water molecules.

In all simulations, periodic boundary conditions were assumed. Short-ranged forces were truncated at half the box length and the Ewald summation method with conducting boundary conditions was applied to account for long-range Coulomb interactions. Further, a Berendsen thermostat [57] was coupled to the system in order to maintain the temperatures under control.

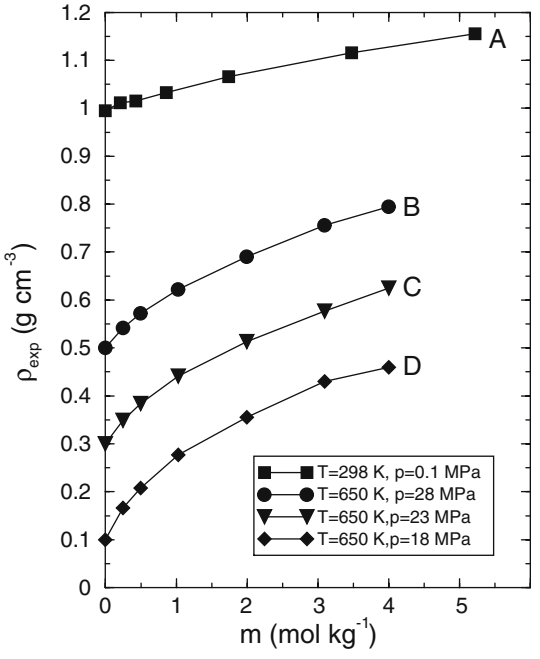

Fig. 1 Experimental densities of ionic solutions at ambient and supercritical conditions as a function of the concentration. Data taken from Refs. [46,47]

3 Structure: radial distribution functions and coordination numbers

Looking at Fig. 1, it is remarkable to observe the large density variations with concentration for the supercritical states (upto factor 4 at the lowest density, state D), whereas the changes at ambient conditions are lower (only upto 15%). The large density changes for SW states would be related to water rearrangements due to the presence of ionic species. The overall structure at supercritical conditions can be roughly visualized with the help of Figs. 2 and 3. There we observe two typical snapshots (using orthographic projection) corresponding to extremal conditions, that is, the first one for the low density state D at low concentration $m = 1\,mol\,kg^{-1}$ (Fig. 2) and the second one for the high density state B at high concentration $m = 4\,mol\,kg^{-1}$ (Fig. 3). A gross feature to be noted is the form of aggregation of the ionic species. In the low-density/low-concentration case, ionic species tend to aggregate in clusters formed by a few ions (say typically 3–6 units), whereas in the case of high-density/high-concentration we can say that ions are homogeneously distributed and

Table 1 Thermodynamic conditions of simulated states and structural properties: radii of the first solvation shells and ion-oxygen coordination numbers

State	T(K)	ρ(g cm^{-3})	m(mol kg^{-1})	R_{Na^+O}(Å)	n_{Na^+O}	R_{Cl^-O}(Å)	n_{Cl^-O}
A	298	1.000	0	3.2	6.0	3.8	7.0
		1.035	1	3.2	5.8	3.9	7.3
		1.070	2	3.2	5.6	3.9	7.3
		1.135	4	3.2	5.1	3.9	7.1
B	650	0.500	0	3.5	5.5	4.5	8.0
		0.620	1	3.5	4.5	4.5	8.1
		0.695	2	3.5	4.3	4.7	9.2
		0.795	4	3.4	3.7	4.9	10.2
C	650	0.300	0	3.5	5.5	4.5	7.5
		0.440	1	3.5	4.0	5.0	10.0
		0.515	2	3.5	3.7	5.5	12.7
		0.625	4	3.4	3.3	5.7	13.4
D	650	0.100	0	3.5	5.0	4.6	7.0
		0.277	1	3.5	3.6	5.5	12.1
		0.355	2	3.4	3.3	5.7	13.5
		0.460	4	3.4	3.2	5.7	13.5

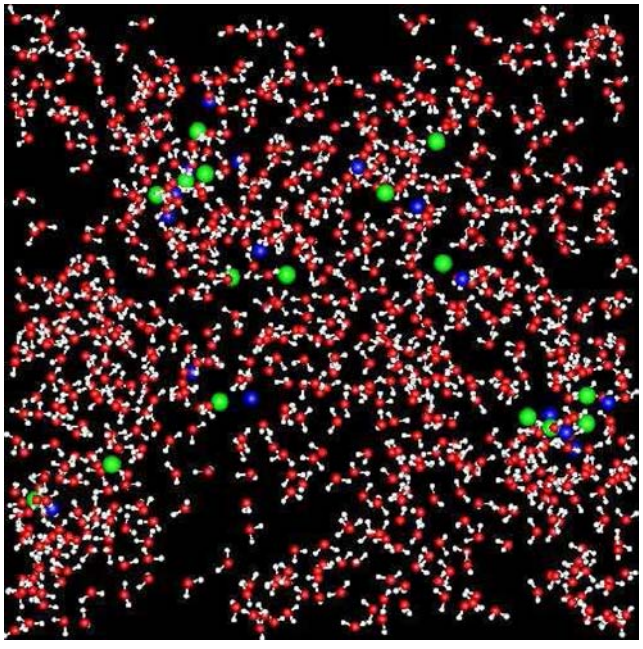

Fig. 2 Snapshot of a typical configuration for state D and $m = 1$ mol kg^{-1}. Oxygens (*red*), hydrogens (*white*), sodium (*blue*), chloride (*green*)

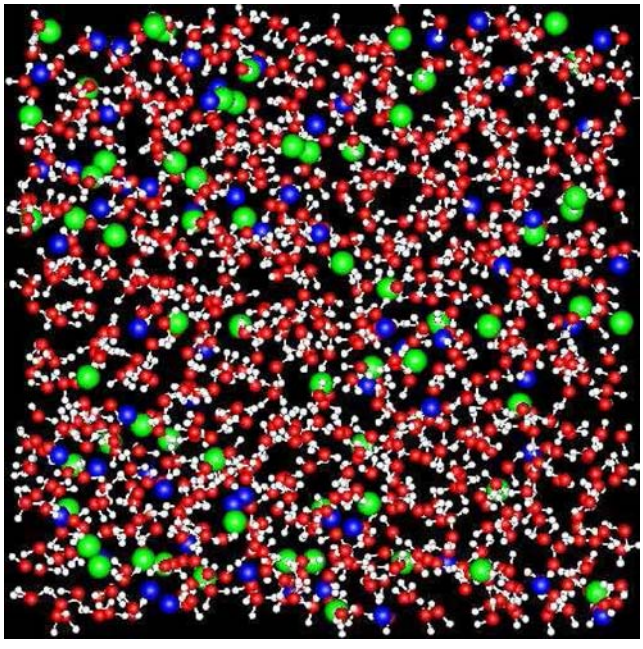

Fig. 3 Snapshot of a typical configuration for state B and $m = 4$ mol kg^{-1}. Colors as in Fig. 2

no neatly distinguishable clustering is observed. This "clustering" effect was also observed by Brodholt [41]. Changes in the structure of the simulated systems will be analyzed in detail from radial distribution functions and coordination numbers.

A set of radial distribution functions $g_{I\alpha}(r)$ can be defined between a given ion I (Ion = Na^+, Cl^-) and species α, where α is either I or O (Oxygen). The $g_{I\alpha}(r)$ functions, which provide a measure of the probability to find a particle α around an ion I at the distance r, have been calculated according to

$$g_{I\alpha}(r) = \frac{V}{N_\alpha}\frac{\Delta n_{I\alpha}(r)}{4\pi r^2 \Delta r} \quad (\alpha = \mathrm{I, O}), \tag{1}$$

where $V = L^3$, L is the box length and $\Delta n_{I\alpha}(r)$ stand for the number of α particles inside a spherical layer of thickness Δr and radius r centered at I.

3.1 Ion-water

In Fig. 4, we show $g_{Na^+O}(r)$ and $g_{Cl^-O}(r)$ at different states. At ambient conditions the structure of water around ions has two well-defined hydration shells (three in the case of chloride) and does not show remarkable changes with concentration. On the contrary, at SW conditions the existence of a second hydration shell is not so clear and ion-water structure is markedly dependent on concentration. As a general

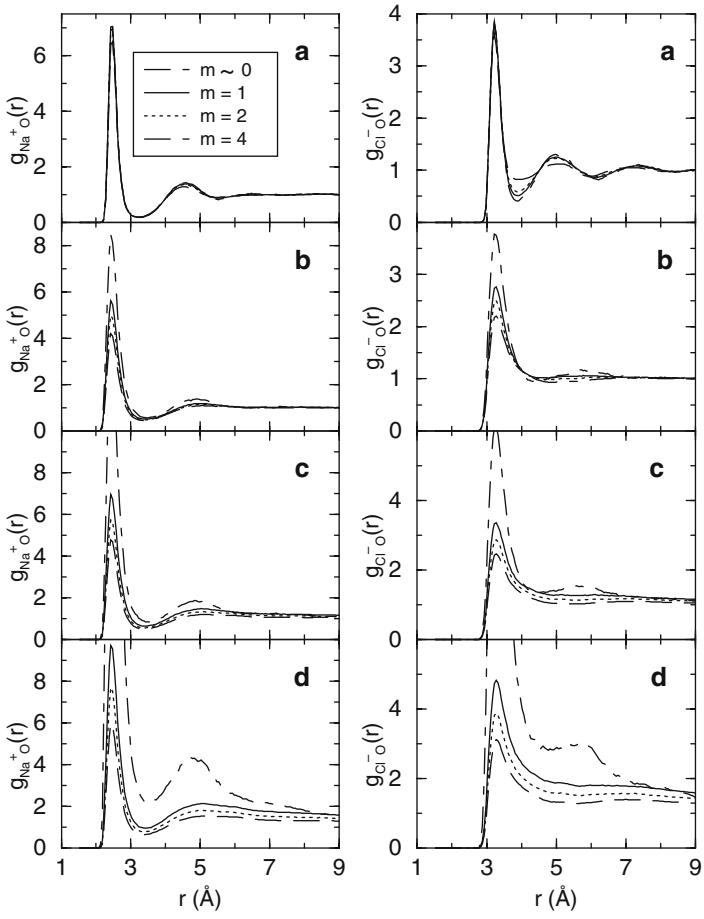

Fig. 4 Ion-oxygen radial distribution functions for states A, B, C and D and different concentrations

trend, the increase in concentration produces a loss of structure. These findings can be attributed to the rather scarce number of water molecules "available" to the ions at supercritical states. Besides, this number tends to decrease as concentration increases. The $g_{Na^+O}(r)$ and $g_{Cl^-O}(r)$ functions at SW conditions reflect a high degree of clustering that becomes more marked as density decreases and concentration increases, which is consistent with the conclusions from the visual inspection of Figs. 2 and 3. The high first maxima of $g(r)$ for infinite dilute systems should be emphasized, specially at low density, which may be attributed to the relatively high proportion of water molecules around the ion. Moreover, in these dilute solutions we can observe a second minimum since there are enough water molecules for a second hydration shell.

Results in Fig. 4 and Table 1 show that the first minima for SW states are well resolved for Na^+ (nearly constant radii $R_{Na^+O} = 3.4$–3.5 Å) but poorly defined for Cl^- (R_{Cl^-O} between 3.9 and 5.7 Å). This should be attributed to differences in the relative orientation between the ion and surrounding water molecules. For Na^+ the oxygen is close to the ion at a fixed distance whereas different relative positions are possible between a Cl^- ion and the close hydrogen atoms of water.

The average number of water molecules in the first solvation shell (coordination numbers, n_{IO}) were obtained by integrating $\Delta n_{I\alpha}(r)$ upto the radius of the shell (R_{IO}), given by the first minimum of $g_{I\alpha}(r)$. The results for n_{IO} and R_{IO} are presented in Table 1. The n_{Na^+O} values decrease as concentration rises and the number of ions to share the actual water molecules becomes higher. Changes with concentration tend to be more marked as density decreases. These findings are consistent with the discussion from the radial distribution functions. The presence of more chloride ions, which tend to approach the sodium ions and occupy some place initially assigned to water molecules favors the decrease of n_{IO} with concentration. The results for the chloride ion at SW conditions are very different since the n_{Cl^-O} values increase as concentration rises and density decreases. This behavior should be attributed to the variety of the radii of the Cl^- hydration shells that unlike for Na^+, show large discrepancies among systems at different states.

3.2 Ion–ion

The radial distribution functions for Na^+Cl^- are presented in Fig. 5. They show two maxima in all cases. The first peak,

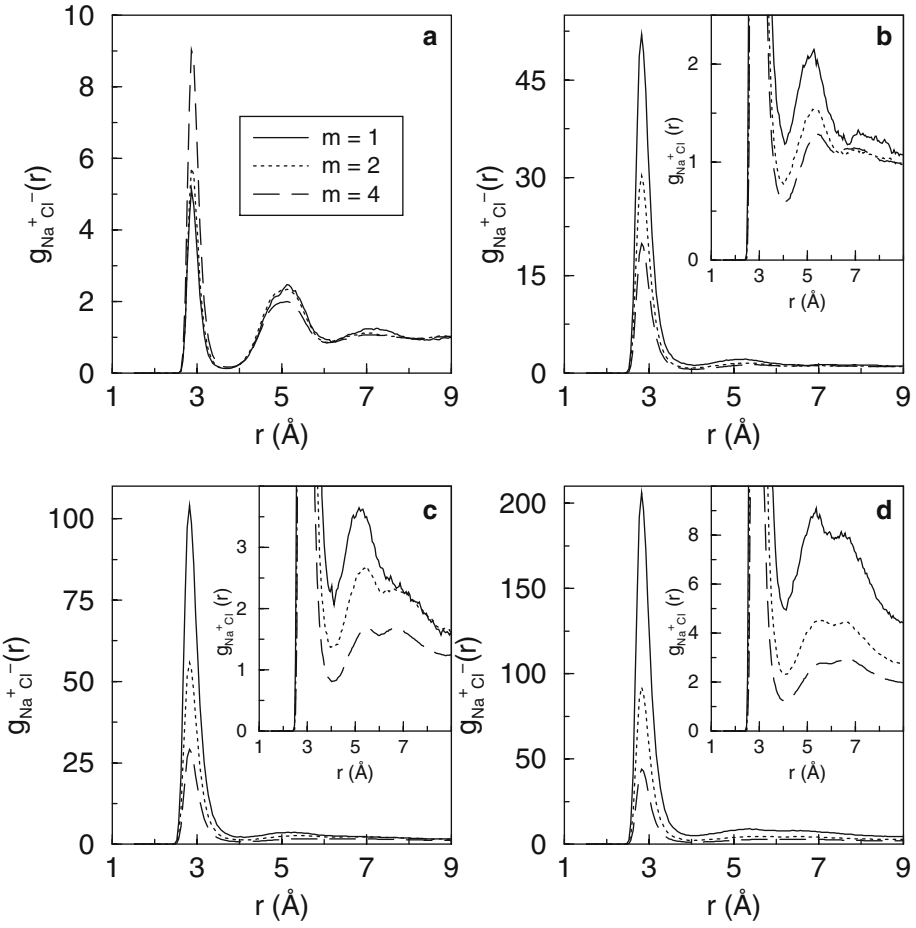

Fig. 5 Sodium chloride radial distribution functions for states A, B, C, D and different concentrations. Insets of the figures display a detail of the regions corresponding to the second coordination shell for supercritical states

at about 1.9 Å, corresponds to contact ion pair configurations whereas the second peak, at about 5.0 Å, corresponds to solvent separated ion pair configurations. These findings are in good agreement with those obtained from constrained MD calculations of the mean force potential for a Na^+Cl^- ion pair in water [23]. The maxima of the $g(r)$ are located at the same positions as the minima of the mean force potential. Two different relative orientations of water molecules between solvent separated ions were observed from constrained MD simulations [23].

A remarkable trend of the $g(r)$ plots in Fig. 5 is the disparity of scales: the higher first maximum for state A shows a height of about 9 units whereas for state D the highest first peak reaches more than 200 units. This is an indication of the great stability of ionic pairs at SW states, stability that increases as density decreases, which is consistent with the commented tendency to clusterization of SW solutions at low densities. Although we can observe a second $g(r)$ maximum for all systems, the ratio height of the second maximum/height of the first maximum shows a sharp reduction when we move from ambient to supercritical conditions. This may be associated with the need for bridging water molecules to configurate the solvent-separated aggregates associated with the second $g(r)$ maximum. Moreover, this ratio decreases as density decreases and the ratio of water molecules and number of ions becomes smaller.

Interesting information on the ion–ion structure is provided by the running coordination numbers $n(r)$ that were obtained by integrating $\Delta n_{I\alpha}(r)$ upto variable distances r. The Na^+Cl^- running coordination numbers are presented in Fig. 6. In all cases the $n(r)$ functions show a clear plateau that reflects the existence of well defined contact ion pairs. It should be noted that for SW systems the average number of contact ion pairs for a tagged ion is in general higher than one, which reflects the existence of ionic clusters at these conditions. $n(r)$ results also reveal a reinforcement of clusterization as density of SW systems decreases. Unlike the manner in which $g(r)$ functions, the coordination numbers of $n(r)$ increase with concentration at both ambient and supercritical conditions. This is an expected result since the largest amount of available ionic counterparts favor the existence of contact ionic pairs. The coordination numbers resulting from this study agree numerically well with those of Brodholt [41].

The radial distribution functions for the Na^+Na^+ pairs are presented in Fig. 7. At ambient conditions, they show a first maximum at about 3.8 Å and a second maximum at

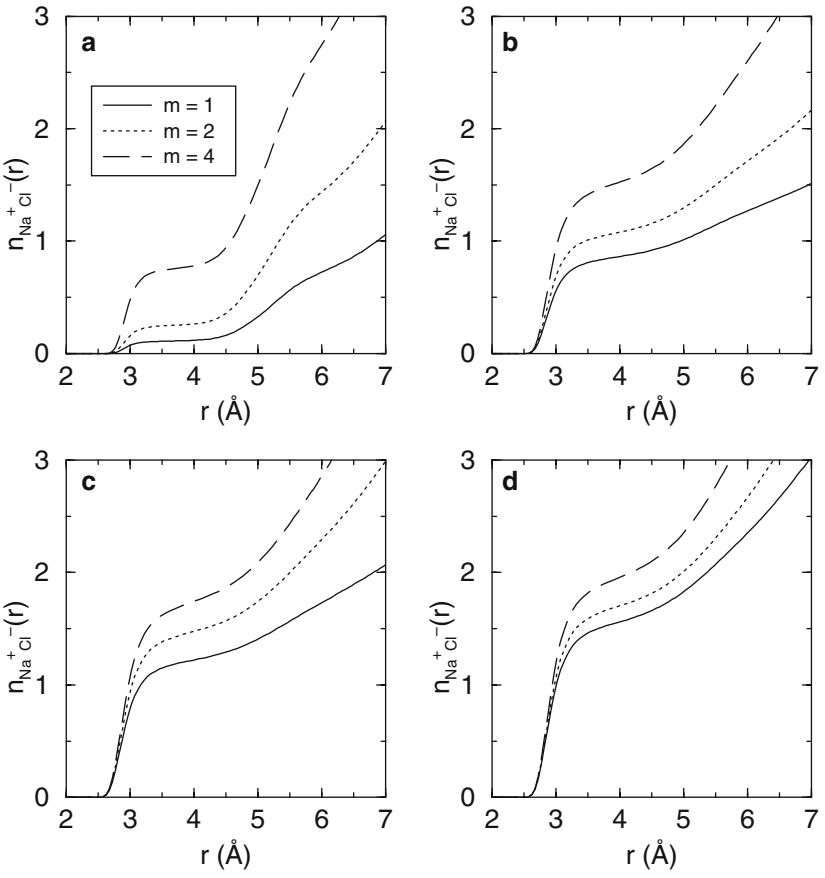

Fig. 6 Sodium chloride running coordination numbers for states A, B, C, D at different concentrations

about 6.0 Å. These results are in very good agreement with the mean force potential for Na^+Na^+ obtained from constrained MD simulations of a single ion pair in water by Guàrdia et al. [24]. According to these findings water molecules surrounding the Na^+Na^+ pairs can stabilize configurations with two ion pairs of the same sign. In the case of the first maximum the oxygen of water molecules serves as a bridge between the two ions whereas the second maximum corresponds to configurations where water molecules are uniformly distributed with the oxygen atoms closer to the Na^+ ions than the hydrogen ones [24]. At SW conditions the $g(r)$ for Na^+Na^+ also show the first maximum at about 3.8 Å. The height of this peak becomes higher at lower densities, which reflects a more marked tendency to clustering. Unlike at ambient conditions the second $g(r)$ maximum cannot be observed for SW states. This may be attributed to the relatively high number of water molecules required to stabilize these configurations.

As with Na^+Na^+, the Cl^-Cl^- radial distribution functions presented in Fig. 8 show the existence of Cl^-Cl^- configurations stabilized by surrounding water molecules. For all simulated systems we found a first $g(r)$ peak located at the same position (at about 5.4 Å) as the minimum of the mean force potential previously obtained from constrained MD simulations of single ion pairs [24]. This should be attributed to configurations with bridging water molecules symmetrically located between the ions whose hydrogen atoms are close to each Cl^-. At ambient conditions we observe a second $g(r)$ peak at about 8.8 Å. This configuration appears for distances longer than those analyzed in earlier mean force calculations [24]. It should correspond to structures with water molecules uniformly distributed between the two ions. A very smooth reminiscent second minimum may be observed for state B, but it is absent for other SW states where the number of available water molecules is rather scarce. As with Na^+Cl^- and Na^+Na^+ the height of the $g(r)$ peaks increases as density decreases, which is consistent with a more marked clustering at low densities and high concentrations.

The radial distribution functions between like ions do not show a deep first minimum close to zero as that for Na^+Cl^-. Then, the first coordination shell is not well defined and the running coordination numbers for Na^+Na^+ and Cl^-Cl^- do not show a clear plateau. This behavior of $n(r)$ may be observed in Fig. 9, where the results for state C are represented. The rest of the states reproduced qualitatively the same trends. This should be attributed to the fact that, unlike Na^+Cl^- contact configurations, ionic pairs of the same sign are stabilized through bridging water molecules and then the range of interionic distances is wider and poorly defined. As it could be expected, $n(r)$ for Na^+Na^+ and Cl^-Cl^- increases

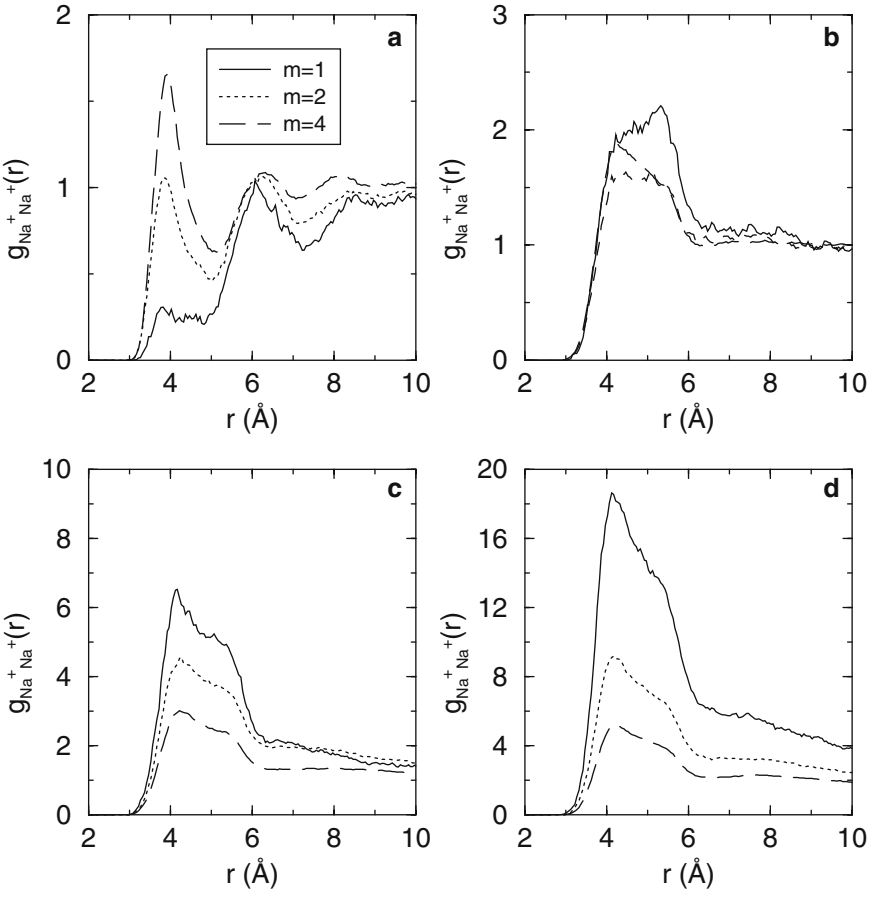

Fig. 7 Sodium–sodium radial distribution functions for states A, B, C, D and different concentrations

with concentration m because of the higher probability to find another ion.

4 Dynamics: residence times

The residence time of water molecules in the first ionic solvation shells has been evaluated by using the procedure described in Ref. [58]. During the simulations, we computed the function $N(t)$, which is defined as the number of molecules that, having initially been in a given solvation shell, remain there after a time t, independently whether they have been outside for any period smaller than t. This function satisfies: $N(0) = n_{IO}$ reported in Table 1. The residence time in the solvation shell τ_I is then determined as the time integral

$$\tau_I = \int_0^\infty \frac{N(t)}{N(0)}\ \mathrm{d}t. \qquad (2)$$

The results for τ_I are presented in Table 2. It should be noted that the residence times for both ionic species at ambient conditions are about one order of magnitude longer than those at SW environments, which corroborates that the water molecules can leave their ionic shells more easily at higher temperatures and lower densities. At supercritical conditions the slight variations of τ_I are mainly related to density changes whereas the influence of the composition is rather weak. This is consistent with the findings of Sherman and Collings [44] who observed a relatively small effect of concentration on ionic self-diffusion coefficients.

At ambient conditions, residence times of water molecules located in the Na^+ hydration shell are clearly higher than those located in the Cl^- shell. This should be related to the differences between the ion-water geometrical configurations for the two ionic species already discussed in Sect. 3.1. Moreover, the stability increases with concentration, which can be a subtle effect of changes in the HB network when water molecules are substituted by ions. When me move to SW ambients the HB network is weaker than that at ambient conditions (see Ref. [59]) and then the influence of the concentration becomes less marked.

5 Concluding remarks

We have presented MD simulations of Na^+ and Cl^- aqueous solutions at different concentrations, from infinite dilution to 4 m. Ambient conditions and supercritical states at 650 K and a range of densities between 0.795 and 0.1 g cm^{-3} selected from fitted experimental data have been considered. We have

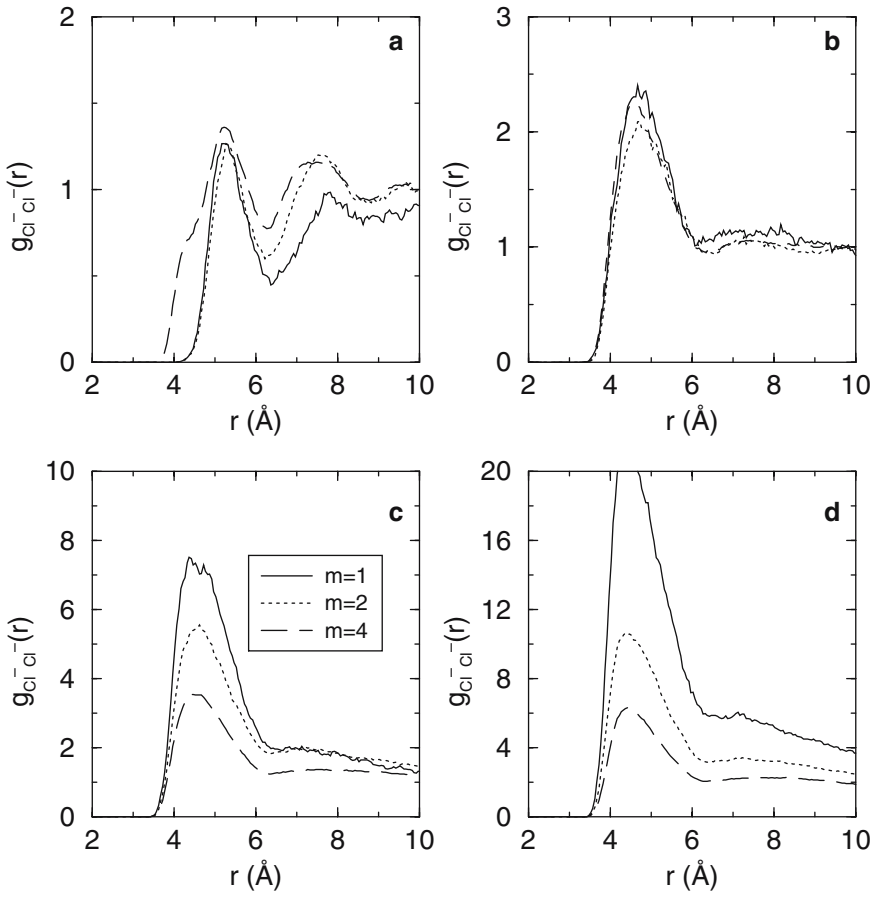

Fig. 8 Chloride–chloride radial distribution functions for states A, B, C, D and different concentrations

Table 2 Residence times of water in the first ionic solvation shells

T (K)	ρ (g cm^{-3})	m (mol kg^{-1})	τ_{Na^+} (ps)	τ_{Cl^-} (ps)
298	1.000	0	25.0	14.0
	1.035	1	22.5	12.0
	1.070	2	24.5	13.4
	1.135	4	31.0	17.0
650	0.500	0	2.7	1.6
	0.620	1	2.2	1.7
	0.695	2	2.2	1.9
	0.795	4	2.2	2.2
650	0.300	0	2.9	1.9
	0.440	1	2.2	2.0
	0.515	2	2.2	2.5
	0.625	4	2.2	2.7
650	0.100	0	3.8	2.6
	0.277	1	2.2	2.4
	0.355	2	2.2	2.6
	0.460	4	2.2	2.9

studied with detail the influence of both density and concentration on microscopic structure and dynamics of these systems.

Ion-water structure has been analyzed upto the second ionic solvation shells. A clear loss of structure is seen when moving from ambient to SW environments. The inspection of radial distribution functions and running coordination numbers indicate a tendency to clustering in supercritical states. We observed significantly different configurations for low (Fig. 2) and high concentrations (Fig. 3). At $m = 1$ mol kg^{-1} the system is formed by "clusters" of solvated ions localized in a given restricted region of the system but, as concentration increases, such solvated ions tend to cover the whole space available.

According to earlier findings at infinite dilution, contact- and solvent-separated Na^+Cl^- ion pairs have been found. Moreover, ion pairs of the same sign stabilized by surrounding water molecules have also been observed at both ambient and supercritical conditions.

Residence times of water molecules at 298 K are one order of magnitude longer than those at SW ambients. However, modifications of the HB network in SW induced by the ionic presence do not produce relevant changes on the values of residence times that are rather independent of concentration.

Acknowledgements The authors gratefully acknowledge financial support from the "Direcció General de Recerca de la Generalitat de Catalunya" (Grant 2001SGR-00222) and the "Ministerio de Educación y Ciencia" of Spain (Grant BFM2003-08211-C03-01). Additional funding by European Union FEDER funds (UNPC-E015) is also acknowledged.

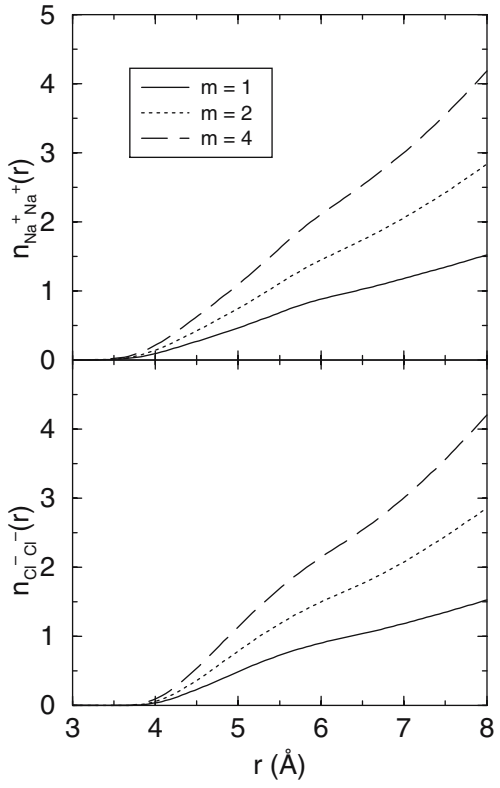

Fig. 9 Sodium–sodium and chloride–chloride running coordination numbers for state C at different concentrations

References

1. Conway BE (1992) Chem Soc Rev 21:253–261
2. Mitton DB, Orzalli JC, Latanision RM (1995) In: White HJ, Sengers JV, Neumann DB, Bellows JC (eds) Physical chemistry of aqueous systems: meeting the needs of industry. Begell House, New York, pp 638–643
3. Shanableh A (2000) Water Res 34:945–951
4. Canganella F, Gambacorta A, Kato C, Horikoshi K (2000) Microbiol Res 154:297–306
5. Mesmer RE, Sweeton FH, Hitch BF, Baes CF (1976) In: Jones DdG, Staehle RW (eds) High temperature high pressure electrochemistry in aqueous solutions. National Association of Corrosion Engineers, Houston, TX, pp 365–374
6. Wood RH, Smith-Magowan D (1980) In: Newman SA (ed) Thermodynamics of aqueous systems with industrial applications, vol. 133. American Chemical Society, Washington, DC, pp 569–581
7. Marshall WL, Frantz JD (1987) In: Ulmer GC, Barnes HL (eds) Hydrothermal experimental techniques, Chap 11. Wiley, New York
8. Walrafen GE (1966) J Chem Phys 44:1546–1558
9. Walrafen GE (1970) J Chem Phys 52:4176–4198
10. Amo Y, Tominaga Y (2000) Physica A 275:33–47
11. Pfund DM, Darab JG, Fulton JL, Ma Y (1994) J Phys Chem 98:13102–13107
12. Wallen SL, Pfund DM, Fulton JL (1998) J Chem Phys 108:4039–4046
13. Ferlat G, San Miguel A, Jal JF, Soetens JC, Bopp PA, Hazemann JL, Testemale D, Daniel I (2002) J Mol Liq 101/1–3:127–136
14. Enderby JE (1995) Chem Soc Rev 24:159–168
15. de Jong PHK, Neilson GW, Bellissent-Funel MC (1996) J Chem Phys 105:5155–5159
16. Yamaguchi T, Yamaguchi M, Ohzono H, Wakita H, Yamanaka K (1996) Chem Phys Lett 252:317–321
17. Kropman MF, Bakker HJ (2001) Science 291:2118–2120
18. Rasaiah JC, Friedman HL (1968) J Chem Phys 48:2742–2752
19. Pratt L, Chandler D (1977) J Chem Phys 67:3683–3704
20. Levesque D, Weis JJ, Patey GN (1980) J Chem Phys 72:1887–1899
21. Pettitt BM, Rossky PJ (1986) J Chem Phys 84:5836–5844
22. Berkowitz M, Karim OA, McCammon JA, Rossky PJ (1984) Chem Phys Lett 105:577–580
23. Guàrdia E, Rey R, Padró JA (1991) Chem Phys 155:187–195
24. Guàrdia E, Rey R, Padró JA (1991) J Chem Phys 95:2823–2831
25. Koneshan S, Rasaiah JC, Lynden-Bell RM, Lee SH (1998) J Phys Chem B 102:4193–4204
26. Chialvo AA, Cummings PT, Simonson JM, Mesmer RE (1999) J Chem Phys 110:1064–1074
27. Driesner T, Cummings PT (1999) J Chem Phys 111:5141–5149
28. Chialvo AA, Kusalik PT, Cummings PT, Simonson JM (2001) J Chem Phys 114:3575–3585
29. Balbuena PB, Johnston KP, Rossky PJ (1996) J Phys Chem 100:2706–2715
30. Balbuena PB, Johnston KP, Rossky PJ (1996) J Phys Chem 100:2716–2722
31. Koneshan S, Rasaiah JC (2000) J Chem Phys 113:8125–8137
32. Koneshan S, Rasaiah JC, Dang LX (2001) J Chem Phys 114:7544–7555
33. Masia M, Rey R (2003) J Phys Chem B 107:2651–2659
34. Anderson J, Ullo J, Yip S (1988) Chem Phys Lett 152:447–452
35. Llano-Restrepo M, Chapman WG (1994) J Chem Phys 100:8321–8339
36. Hummer G, Soumpasis DM, Neumann M (1994) J Phys Condens Matter 6:A141–A144
37. Chandra A (2000) Phys Rev Lett 85:768–771
38. Chandra A (2000) J Chem Phys 113:903–905
39. Chowdhuri S, Chandra A (2001) J Chem Phys 115:3732–3741
40. Oelkers EH, Helgeson HC (1993) Science 261:888–891
41. Brodholt JP (1998) Chem Geol 151:11–19
42. Driesner T, Seward TM, Tironi IG (1998) Geochim et Cosmochim Acta 62:3095–3197
43. Reagan MT, Harris JG, Tester JW (1999) J Phys Chem B 103:7935–7941
44. Sherman DM, Collings MD (2002) Geochem Trans 3:102–107
45. Eckert CA, Knutson BL, Debenedetti PG (1996) Nature (Lond) 383:313–318
46. Archer DG (1992) J Phys Chem Ref Data 21:793–829
47. Majer V, Hui L, Crovetto R, Wood RH (1991) J Chem Thermodyn 23:213–229
48. Berendsen HJC, Grigera JR, Straatsma TP (1987) J Phys Chem 91:6269–6271
49. Guillot B, Guissani Y (1993) J Chem Phys 98:8221–8235
50. Bellissent-Funel MC, Tassaing T, Zao H, Beysens D, Guillot B, Guissani Y (1997) J Chem Phys 107:2942–2949
51. Rønne C, Thrane L, Åstrand PO, Wallqvist A, Mikkelsen KV, Keiding SR (1997) J Chem Phys 107:5319–5331
52. Guàrdia E, Martí J (2004) Phys Rev E 69:011502
53. Guàrdia E, Martí J, García-Tarrés L, Laria D (2005) J Mol Liq 117:63–67
54. Lee SH, Rasaiah JC (1996) J Phys Chem 100:1420–1425
55. Rasaiah JC, Noworyta JP, Koneshan S (2000) J Am Chem Soc 122:11182–11193
56. Noworyta JP, Koneshan S, Rasaiah JC (2000) J Am Chem Soc 122:11194–11202
57. Berendsen HJC, Postma JPM, van Gunsteren WF, DiNola A, Haak JR (1984) J Chem Phys 81:3684–3690
58. Impey RW, Madden PA, McDonald IR (1983) J Phys Chem 87:5071–5083
59. Martí J (1999) J Chem Phys 110:6876–6886